ORGANIC CHEMISTRY

Boron-enabled geometric isomerization of alkenes via selective energy-transfer catalysis

John J. Molloy*†, Michael Schäfer†, Max Wienhold, Tobias Morack, Constantin G. Daniliuc, Ryan Gilmour*

Isomerization-based strategies to enable the stereodivergent construction of complex polyenes from geometrically defined alkene linchpins remain conspicuously underdeveloped. Mitigating the thermodynamic constraints inherent to isomerization is further frustrated by the considerations of atom efficiency in idealized low–molecular weight precursors. In this work, we report a general ambiphilic C_3 scaffold that can be isomerized and bidirectionally extended. Predicated on highly efficient triplet energy transfer, the selective isomerization of β-borylacrylates is contingent on the participation of the boron p orbital in the substrate chromophore. Rotation of the C(sp^2)–B bond by 90° in the product renders re-excitation inefficient and endows directionality. This subtle stereoelectronic gating mechanism enables the stereocontrolled syntheses of well-defined retinoic acid derivatives.

Complex polyenes provide an expansive structural framework for biological processes that occur in two-dimensional chemical space (*1*), yet synthetic paradigms that enable the stereocontrolled construction of these motifs remain conspicuous in their absence. In the biochemical context, information is stored in one of two stereoisomeric forms, such that the spatiotemporal control of constituent alkene units encodes for a specific biological function (*2*–*4*). In cross-conjugated alkenes such as retinal (vitamin A), this interplay facilitates the regulatory gating mechanism that underpins the mammalian visual cycle (*5*). Despite powerful manifestations of this structure-function interplay in human medicine and materials research, isomerization platforms that enable the stereodivergent construction of complex polyenes from common linchpins remain underdeveloped. Synthesis algorithms reported by Burke and co-workers have greatly facilitated the modular construction of polyenes from common building blocks in a manner that is reminiscent of biopolymer assembly (*6*, *7*). Despite these advances, the intractable challenges that are associated with inverting the geometry of small alkene fragments to enable stereodivergence from common precursors offer the opportunity for creative endeavor (*8*). This

Organisch-Chemisches Institut, Westfälische Wilhelms-Universität Münster, Corrensstraße 36, 48149 Münster, Germany.
***Corresponding author. Email: molloy@uni-muenster.de (J.J.M.); ryan.gilmour@uni-muenster.de (R.G.)** †These authors contributed equally to this work.

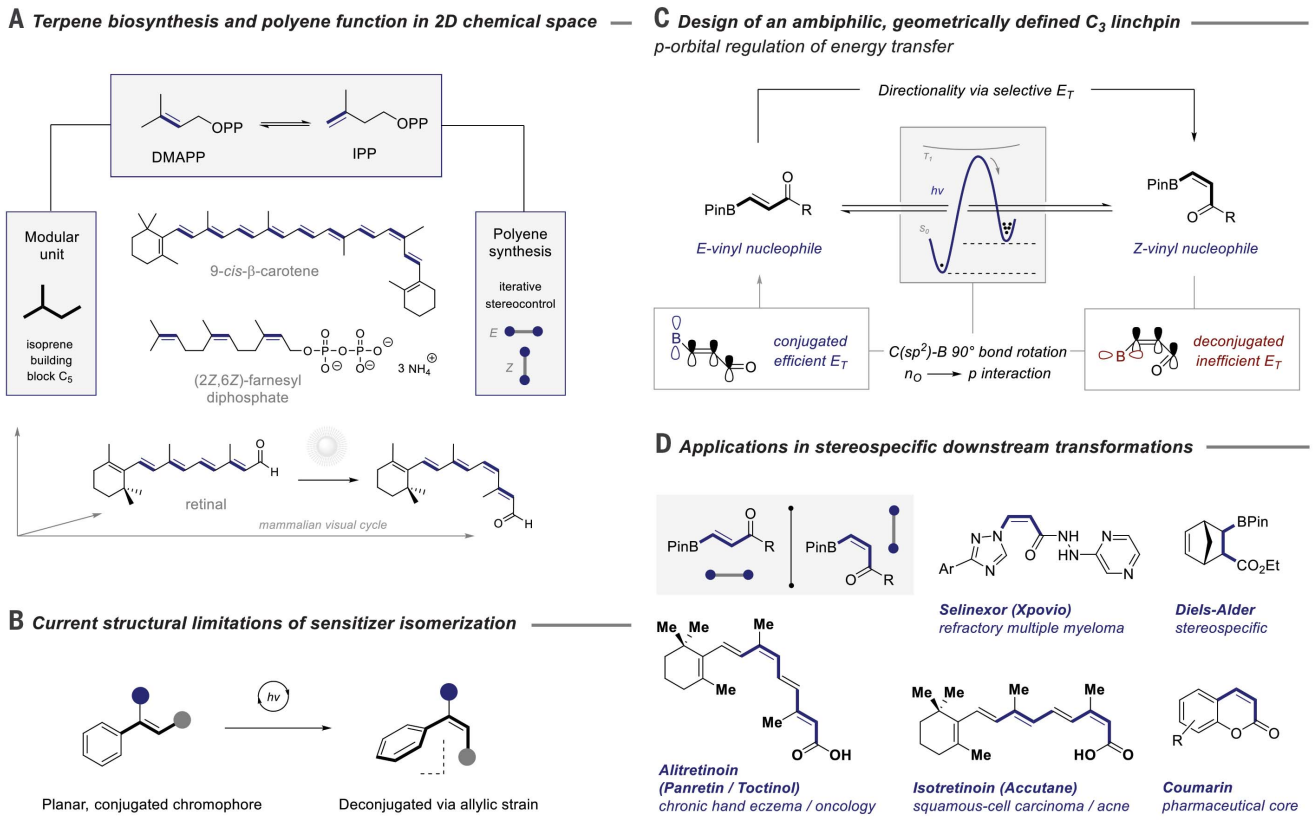

Fig. 1. Inspiration for the development of a photocatalytic isomerization. (**A**) The biosynthesis of complex terpenes via well-defined building blocks and the importance of alkene geometry in the visual cycle. 2D, two-dimensional; OPP, pyrophosphate; DMAPP, dimethylallyl pyrophosphate; IPP, isopentenyl pyrophosphate. (**B**) Photosensitized isomerization of alkenes and the precondition that the alkene is embedded in a larger chromophore (e.g., styrene). hν, photon energy. (**C**) Design of an ambiphilic C_3 linchpin. Selective energy-transfer (E_T) platform is based on the β-boryl-acrylate scaffold. (**D**) Stereospecific applications of the geometrically defined linchpins for the preparation of complex polyenes and pharmaceuticals. The stereochemical assignment of the alkene fragment follows International Union of Pure and Applied Chemistry (IUPAC) nomenclature and reflects the priority order C > B > H.

strategic deficiency in alkene isomerization technology has been highlighted by Baran and co-workers in the context of accessing dienophiles for cycloaddition chemistry (*9*). Terpene biosynthesis predicated on the sequential elongation of small (C5) alkene-containing linchpins such as DMAPP and IPP is a conceptually attractive blueprint in reconciling this disparity (Fig. 1A) (*10*–*12*). Under the auspices of enzyme catalysis, these fragments are unified with high fidelity, thereby enabling the synthesis of well-defined polyenes by either stereodivergent biosynthesis (e.g., farnesyl diphosphate) or postproduct isomerization routes (e.g., 9-*cis*-β-carotene) (*13*). Although challenging to implement in a synthetic context, these precedents highlight the need for an isomerization platform to enable stereodivergent access to both alkene geometries as a prerequisite for efficiency (*14*). Consideration of step and atom economy (*15*) necessitates the use of a common ambiphilic building block that contains the minimum number of carbon atoms needed for sequential manipulation to allow stereospecific downstream processing. The nondegeneracy of alkene stereoisomers and the associated contra-thermodynamic challenges render Dexter-type energy-transfer activation (*16*–*21*) ideally suited to mitigate microscopic reversibility that is intrinsic to ground state reactivity (*22*–*24*). Furthermore, the biocompatibility of this activation strategy has recently been validated by MacMillan and co-workers (*25*).

Photosensitized alkene isomerization has a venerable history, but efficiency often restricts

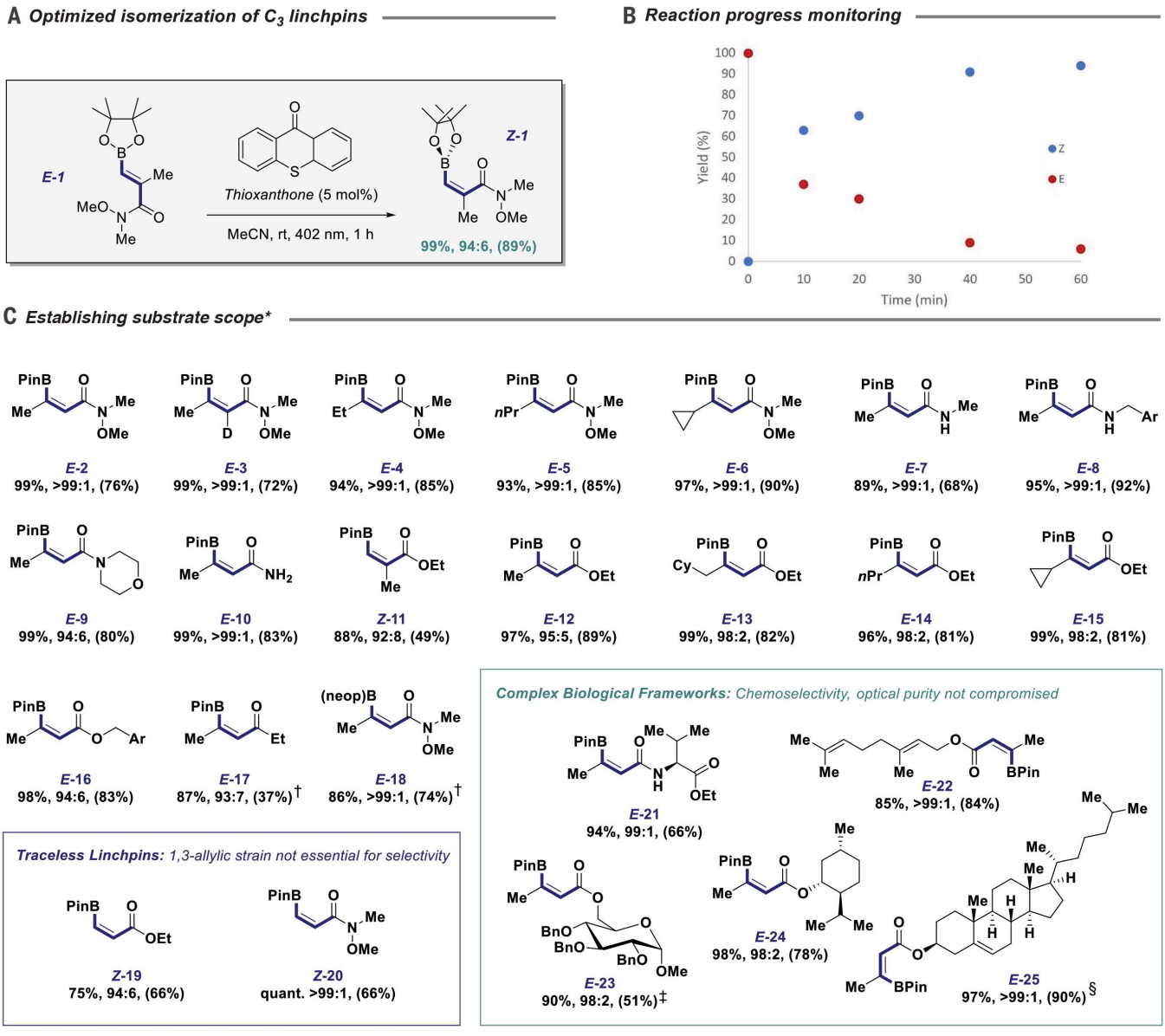

Fig. 2. The photocatalytic isomerization of small molecule ambiphilic C3 linchpins. (**A**) Optimized reaction conditions: substrate (0.3 mmol), thioxanthone (5 mol %), MeCN (9 mL), 402 nm light, 1 hour. rt, room temperature. (**B**) Reaction progress monitoring of ***E*-1** → ***Z*-1**. (**C**) Establishing substrate scope and demonstrating efficiency in simple 1,2-disubstituted systems, showing chemoselectivity and compatibility with biomolecules.

*The stereochemical assignment of the alkene fragment follows IUPAC nomenclature and reflects the priority C > B > H. †Yield over two steps after cross-coupling. ‡0.1 mmol scale. §16 hours. Yields and *E*:*Z* ratios were determined by ^{1}H NMR integration (using 1,3,5-trimethoxybenzene as internal standard). Numbers in parentheses refer to isolated yields of the major product isomer after column chromatography. quant., quantitative.

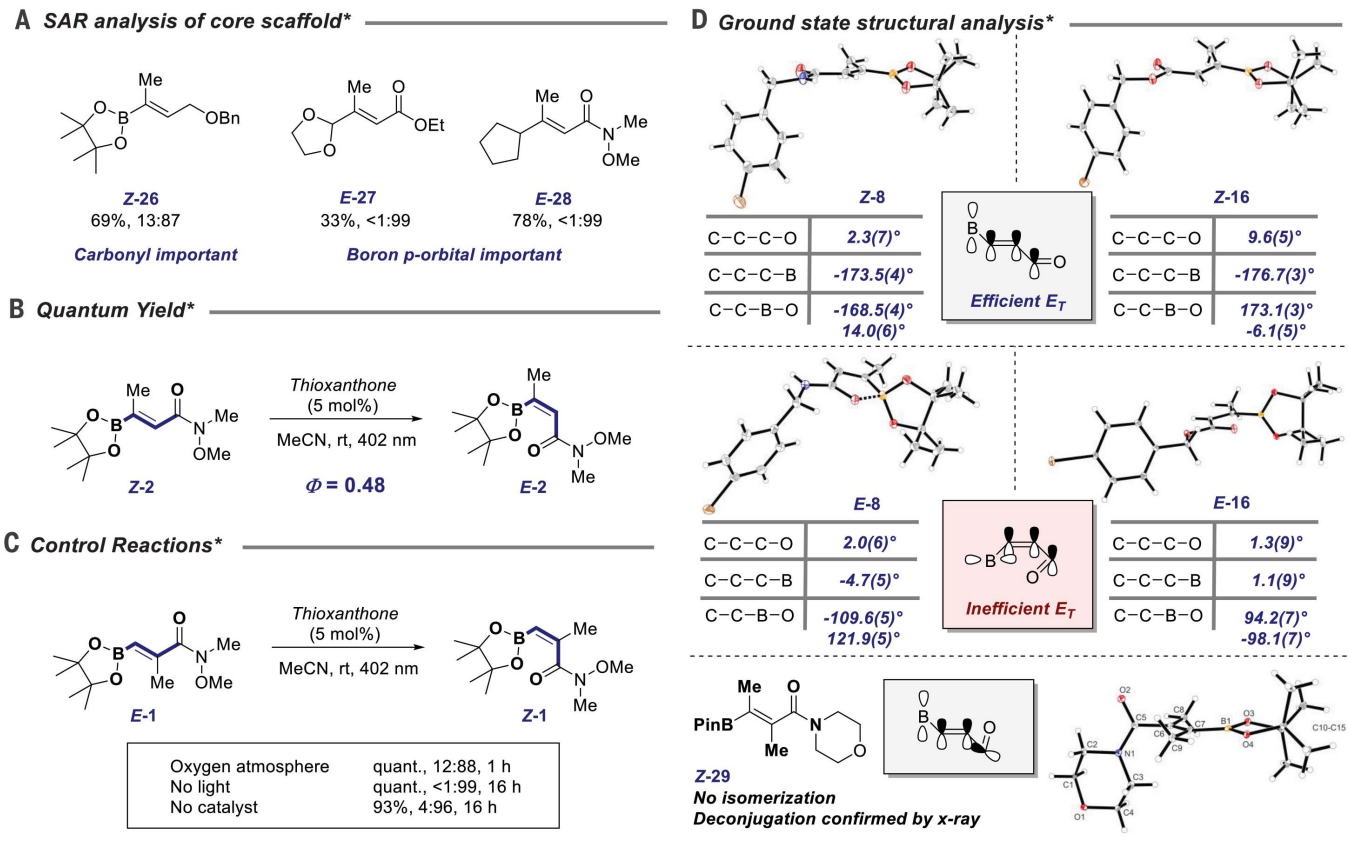

Fig. 3. Investigating the origin of stereoselectivity. (**A**) Structure activity relationship (SAR) of core scaffold. (**B**) Quantum yield studies. (**C**) Control reactions. (**D**) Ground state x-ray structural analysis of ***Z/E*-8**, ***Z/E*-16**, and ***Z*-29**. *The stereochemical assignment of the alkene fragment follows IUPAC nomenclature and reflects the priority C > B > H.

the scope to styrenyl chromophores (*3*). Seminal studies by Hammond *et al.* and Arai *et al.* have established benchmarks for stilbene and styrene isomerization through the use of a photosensitizer (*26*–*29*), and Walker and Radda have simulated triplet energy transfer–enabled selective isomerization of retinal in the visual cycle (*30*). More recently, the Weaver group (*31*) and our own research group (*32*–*35*) have disclosed operationally simple isomerization protocols that harness functionally diverse styrenes with various structural motifs in the β-position (Fig. 1B). However, the presence of an aryl alkene fragment is a precondition to act as a suitable chromophore. Thus, the identification of a traceless chromophore would represent a notable advance toward achieving operational parity with positional isomerization (*36*).

To circumvent this limitation and enable a modular assembly of polyenes (*6*–*8*, *37*) with sequential control of alkene geometry, we consolidated the importance of acetyl derivatives in biosynthesis and the need for an ambiphilic fragment in the β-borylacrylate scaffold (Fig. 1C). Specifically, we identified the boronic acid pinacol ester (β-BPin) as a group that might enable isomerization to generate both alkene isomers and provide a handle for traceless, stereospecific coupling. The conceptual framework of the alkene isomerization was predicated on rotation of the C(sp^2)–B bond as a stereoelectronic gating mechanism to enable selective energy transfer. The p orbital of trigonal planar boron systems plays a pivotal role in regulating the reactivity of organoboron compounds (*38*, *39*). We envisaged that the incorporation of a traceless boronic ester motif as an aryl surrogate would extend the acrylate chromophore and permit subsequent excitation of the planar *E* isomer. After excitation and subsequent isomerization, the C(sp^2)–B bond in the product *Z* isomer would be twisted by 90° and could potentially engage in a dative interaction with the carbonyl group ($n_O \rightarrow p$) (*40*, *41*). This subtle bond rotation would shorten the chromophore and provide a structural foundation to bias the photostationary composition.

In this work, we report a photocatalytic isomerization of β-borylacrylate derivatives that enables access to both geometric isomers of ambiphilic C_3 linchpins. Whereas hydroboration provides a convenient platform to generate a single alkene isomer, this approach harnesses Dexter-type selective energy transfer using an inexpensive small molecule photosensitizer (excited at 402 nm) to enable stereodivergence. Directionality ($E \rightarrow Z$) is a consequence of a subtle 90° C(sp^2)–B bond rotation, thereby contracting the π system of the *Z* isomer. This strategy circumvents the reliance of alkene isomerization on styrenyl chromophores by replacing inert aryl rings with a traceless BPin handle. Both isomers of the vinyl boron species are compatible with stereospecific cross-coupling, which provides the basis for an iterative, stereodivergent entry to complex polyenes. Mechanistic validation and the total syntheses of the therapeutics isotretinoin and alitretinoin are disclosed, and we showcase the synthetic utility of these small, densely functionalized units in stereospecific transformations (Fig. 1D).

Initially, we investigated the geometric isomerization of the ambiphilic Weinreb amide ***E*-1** to ***Z*-1** (Fig. 2A and supplementary materials). Reactions performed in acetonitrile under visible light irradiation (402 nm) using thioxanthone as a photocatalyst (5 mol %) proved to be operationally simple and highly

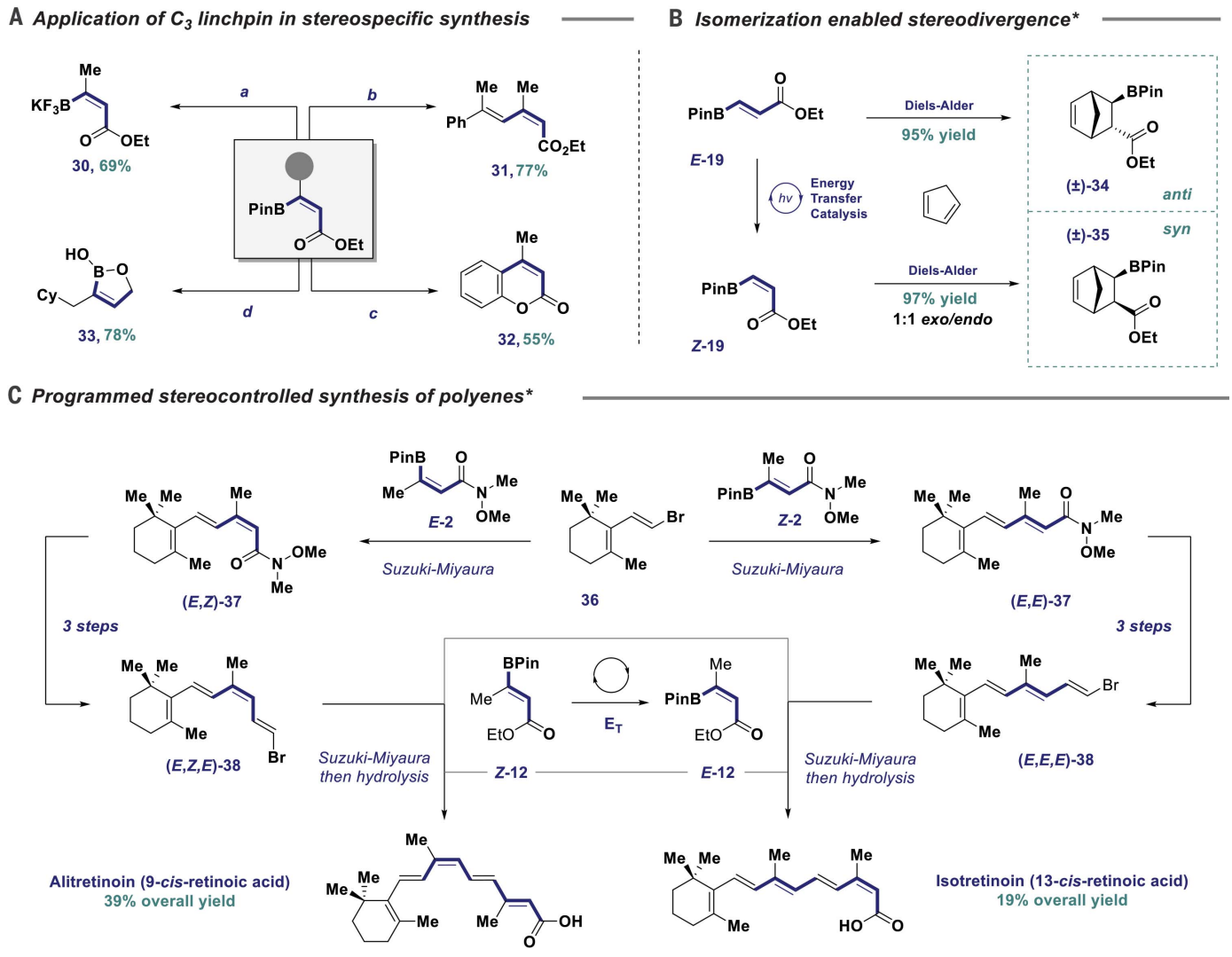

Fig. 4. Stereospecific and stereodivergent application of small molecule C_3 linchpins. (**A**) Application of product isomer in synthesis: (a) ***E*-12** (1 equiv), aq. KHF_2 (4.5 M, 5 equiv), MeOH, rt. (b) ***E*-12** (1 equiv), $Pd(OAc)_2$ (5 mol %), SPhos (10 mol %), K_3PO_4 (3 equiv), vinyl halide (1.2 equiv), H_2O (5 equiv), 1,4-dioxane, 80°C. (c) ***E*-12** (1 equiv), $Pd(OAc)_2$ (5 mol %), SPhos (10 mol %), K_3PO_4 (3 equiv), 2-bromophenol (1.2 equiv), H_2O (5 equiv), 1,4-dioxane, 80°C. (d) ***E*-13** (1 equiv), $NaBH_4$ (2 equiv), rt. (**B**) Stereodivergent Diels-Alder reaction: toluene, 16 hours. (**C**) Stereocontrolled synthesis of the polyene pharmaceuticals alitretinoin (9-*cis*-retinoic acid) and isotretinoin (13-*cis*-retinoic acid). Full details are provided in the supplementary materials. *The stereochemical assignment of the alkene fragment follows IUPAC nomenclature and reflects the priority C > B > H.

efficient [99% nuclear magnetic resonance (NMR) yield, *Z*:*E* = 94:6; Fig. 2, A and B]. With these optimized conditions, we explored the substrate scope and limitations of the method (Fig. 2C). Relocating the methyl substituent to the β-position of the Michael acceptor ***E*-2** and ***E*-3** led to notable selectivity (>99:1). Modification of the alkyl substituent was very well tolerated, furnishing the isomerized products in >99:1 selectivity and with high isolated yields (***E*-4**, ***E*-5**, and ***E*-6**).

Replacement of the Weinreb amide by secondary amides (***E*-7** and ***E*-8**), tertiary amides (***E*-9**), and primary carboxamides (***E*-10**) had no impact on the efficiency of the transformation (up to >99:1). Ester groups were also found to be compatible with the general isomerization conditions, but the α-substituted Michael acceptor (***Z*-11**) proved to be unstable toward silica gel chromatography. High levels of stereoselectivity and isolated yield were also observed with β-substituted analogs (***E*-12** to ***E*-16**, up to 98:2). Efficient isomerization was observed with ketones and neopentyl boronic esters (***E*-17** and ***E*-18**, 93:7 and >99:1, respectively), but the intrinsic instability of the products required a cross-coupling protocol after isomerization to determine stereoselectivity. To explore the limitations of the method in simple 1,2-disubstituted frameworks, we investigated acrylates **19** and **20**. Photochemical alkene isomerization typically requires a substituent to generate 1,3-allylic strain in the product, thereby causing deconjugation, reducing the efficiency of energy transfer, and enabling directionality. In contrast to styrenyl systems, the isomerization of the basic β-borylacrylate also occurs with high levels of stereoselectivity (***E*-19** and ***E*-20**, 94:6 and >99:1, respectively), which provides entry to simple 1,2-disubstituted ambiphilic linchpins. To ensure that the method does not compromise optical purity and is compatible with preexisting alkenes (thereby demonstrating chemoselectivity), we prepared **21** and **22**, respectively. Finally, extension of

the scope to common, biologically relevant frameworks included D-glucose derivative **23**, the (–)-menthol derivative **24**, and modified cholesterol **25** (up to >99:1).

The efficiency of isomerization using simple 1,2-disubstituted building blocks such as **19** and **20** indicates that stereoselectivity is not contingent on allylic strain as is observed with styrenyl systems. To discern the structural basis of the selectivity, we investigated the effects of single-site editing on the core substrate (Fig. 3A). These investigations revealed that both the boron and the carbonyl substituent are critical to achieve efficient directionality, as is clear from ***E*-26**, **27**, and **28**. Determination of the quantum yield excludes the possibility of an efficient radical chain process, and control experiments demonstrate the need for both light and a photocatalyst (Fig. 3, B and C). In establishing the structural basis of directionality, inspection of the ^{11}B NMR spectra of the products proved instructive. Accumulation of electron density in the boron p orbital is conspicuous in the product *E* isomer of the amide derivatives [17.19 ppm (parts per million) for ***E*-8**]. This is indicative of a stabilizing dative ($n_O \rightarrow p$) interaction that is only geometrically viable when the C(sp^2)–B bond rotates out of the plane of the π-system (fig. S6). This deconjugative contraction of the chromophore does not manifest itself in the ^{11}B NMR spectra of the ester substrates (30.76 ppm for ***E*-16**), which prompted further investigation.

It was possible to analyze the substrate and product antipodes of **8** and **16** by x-ray crystallography (Fig. 3D). Comparison of the starting isomers ***Z*-8** and ***Z*-16** confirmed the expected planar chromophore in which the boron group is conjugated (Fig. 3D, top). Consistent with the ^{11}B NMR studies, a clear dative interaction is evident in the amide product ***E*-8** resulting from a 90° rotation of the C(sp^2)–B bond (Fig. 3D, middle). This subtle contraction of the π-system would likely raise the triplet energy and render re-excitation inefficient. The ester derivative ***E*-16** shows no dative interaction, but, consistent with the amide scenario, the boron p orbital is perpendicular to the alkene π-system and no longer in conjugation. To further demonstrate the importance of conjugation for efficient sensitization, the *tetra*-substituted precursor ***Z*-29** was investigated. X-ray analysis revealed that the carbonyl group is out of plane, thereby rendering excitation inefficient. Although *tetra*-substituted alkenes are seldom found in polyenes, this substrate is a useful control.

To validate this isomerization platform in stereocontrolled polyene synthesis, we investigated the synthetic utility of simple ambiphilic linchpins in target synthesis and a series of downstream manipulations (Fig. 4). Boronic ester protection to generate the corresponding trifluoroborate was facile (**30**; Fig. 4A). Similarly, stereospecific cross-coupling to form diene **31** with alternating geometrical isomers proceeded in high yields, whereas the use of 2-bromo phenol allowed the rapid generation of the coumarin scaffold **32**. A known covalent binder in medicinal chemistry, the oxaborole scaffold (**33**) could be accessed by standard reduction conditions. Isomerization enabled stereodivergent Diels-Alder reactions to generate the *anti*-adduct **34** and the *syn*-adduct **35** (Fig. 4B). Our ultimate goal was to enable the programmed, stereocontrolled synthesis of polyenes by using simple, geometrically defined alkenes (Fig. 4C). Using easily accessible vinyl bromide **36**, stereospecific cross-coupling using (*Z*)- and (*E*)-**2** allowed expedient access to geometrical isomers (*E*, *E*)- and (*E*, *Z*)-**37** in high yield and selectivity. Subsequent reduction to the aldehyde—using the boron-Wittig reaction, as developed by Morken and coworkers (*42*)—followed by bromodeboronation furnished stereodefined vinyl bromide intermediate (*E*, *E*, *E*)- and (*E*, *Z*, *E*)-**38** (see supplementary materials for full details). Suzuki-Miyaura cross-coupling (*43*–*45*) with ***E*-12** proceeded smoothly to furnish 13-*cis*-retinoic acid (isotretinoin) after subsequent hydrolysis. The analogous sequence with ***Z*-12** enabled the synthesis of 9-*cis*-retinoic acid (alitretinoin) (*46*). This platform for the stereocontrolled generation of complex polyenes might prove to be expansive and may facilitate the exploration of these bioactive materials in drug discovery.

REFERENCES AND NOTES

1. C. Dugave, L. Demange, *Chem. Rev.* **103**, 2475–2532 (2003).
2. C. M. Pearson, T. N. Snaddon, *ACS Cent. Sci.* **3**, 922–924 (2017).
3. J. J. Molloy, T. Morack, R. Gilmour, *Angew. Chem. Int. Ed.* **58**, 13654–13664 (2019).
4. L. F. Maia, R. F. Fernandes, G. Lobo-Hajdu, L. F. C. de Oliveira, *Phil. Trans. R. Soc. A* **372**, 20140200 (2014).
5. P. D. Kiser, M. Golczak, K. Palczewski, *Chem. Rev.* **114**, 194–232 (2014).
6. E. M. Woerly, J. Roy, M. D. Burke, *Nat. Chem.* **6**, 484–491 (2014).
7. S. J. Lee, K. C. Gray, J. S. Paek, M. D. Burke, *J. Am. Chem. Soc.* **130**, 466–468 (2008).
8. J. W. Lehmann, D. J. Blair, M. D. Burke, *Nat. Rev. Chem.* **2**, 0115 (2018).
9. T.-G. Chen *et al*., *Nature* **560**, 350–354 (2018).
10. A. Eschenmoser, L. Ruzicka, O. Jeger, D. Arigoni, *Helv. Chim. Acta* **38**, 1890–1904 (1955).
11. A. Eschenmoser, D. Arigoni, *Helv. Chim. Acta* **88**, 3011–3050 (2005).
12. J. W. Cornforth, *Pure Appl. Chem.* **2**, 607–630 (1961).
13. G. W. Burton, K. U. Ingold, *Science* **224**, 569–573 (1984).
14. B. M. Trost, *Science* **219**, 245–250 (1983).
15. B. M. Trost, *Science* **254**, 1471–1477 (1991).
16. M. Kathan, S. Hecht, *Chem. Soc. Rev.* **46**, 5536–5550 (2017).
17. R. S. Stoll, S. Hecht, *Angew. Chem. Int. Ed.* **49**, 5054–5075 (2010).
18. M. Kathan *et al*., *Nat. Chem.* **10**, 1031–1036 (2018).
19. A. Hölzl-Hobmeier *et al*., *Nature* **564**, 240–243 (2018).
20. E. Ota, H. Wang, N. L. Frye, R. R. Knowles, *J. Am. Chem. Soc.* **141**, 1457–1462 (2019).
21. N. Y. Shin, J. M. Ryss, X. Zhang, S. J. Miller, R. R. Knowles, *Science* **366**, 364–369 (2019).
22. F. Strieth-Kalthoff, M. J. James, M. Teders, L. Pitzer, F. Glorius, *Chem. Soc. Rev.* **47**, 7190–7202 (2018).
23. L. Marzo, S. K. Pagire, O. Reiser, B. König, *Angew. Chem. Int. Ed.* **57**, 10034–10072 (2018).
24. Q.-Q. Zhou, Y.-Q. Zou, L.-Q. Lu, W.-J. Xiao, *Angew. Chem. Int. Ed.* **58**, 1586–1604 (2019).
25. J. B. Geri *et al*., *Science* **367**, 1091–1097 (2020).
26. G. S. Hammond, J. Saltiel, *J. Am. Chem. Soc.* **84**, 4983–4984 (1962).
27. G. S. Hammond *et al*., *J. Am. Chem. Soc.* **86**, 3197–3217 (1964).
28. T. Arai, H. Sakuragi, K. Tokumaru, *Chem. Lett.* **9**, 261–264 (1980).
29. T. Arai, H. Sakuragi, K. Tokumaru, *Bull. Chem. Soc. Jpn.* **55**, 2204–2207 (1982).
30. A. G. Walker, G. K. Radda, *Nature* **215**, 1483 (1967).
31. K. Singh, S. J. Staig, J. D. Weaver, *J. Am. Chem. Soc.* **136**, 5275–5278 (2014).
32. J. B. Metternich, R. Gilmour, *J. Am. Chem. Soc.* **137**, 11254–11257 (2015).
33. J. B. Metternich, R. Gilmour, *J. Am. Chem. Soc.* **138**, 1040–1045 (2016).
34. J. J. Molloy, J. B. Metternich, C. G. Daniliuc, A. J. B. Watson, R. Gilmour, *Angew. Chem. Int. Ed.* **57**, 3168–3172 (2018).
35. S. I. Faßbender, J. J. Molloy, C. Mück-Lichtenfeld, R. Gilmour, *Angew. Chem. Int. Ed.* **58**, 18619–18626 (2019).
36. A. Vasseur, J. Bruffaerts, I. Marek, *Nat. Chem.* **8**, 209–219 (2016).
37. M. Burns *et al*., *Nature* **513**, 183–188 (2014).
38. A. J. J. Lennox, G. C. Lloyd-Jones, *Chem. Soc. Rev.* **43**, 412–443 (2014).
39. D. G. Hall, Ed., *Boronic Acids* (Wiley, 2011).
40. R. J. Grams, R. G. Fritzemeier, C. Slebodnick, W. L. Santos, *Org. Lett.* **21**, 6795–6799 (2019).
41. K. Nagao, A. Yamazaki, H. Ohmiya, M. Sawamura, *Org. Lett.* **20**, 1861–1865 (2018).
42. J. R. Coombs, L. Zhang, J. P. Morken, *Org. Lett.* **17**, 1708–1711 (2015).
43. N. Schneider, D. M. Lowe, R. A. Sayle, M. A. Tarselli, G. A. Landrum, *J. Med. Chem.* **59**, 4385–4402 (2016).
44. J. W. B. Fyfe, A. J. B. Watson, *Chem* **3**, 31–55 (2017).
45. A. J. J. Lennox, G. C. Lloyd-Jones, *Angew. Chem. Int. Ed.* **52**, 7362–7370 (2013).
46. S. Khalil *et al*., *J. Dermatolog. Treat.* **28**, 684–696 (2017).

ACKNOWLEDGMENTS

This work is dedicated to the memory of Dr. Duilio Arigoni. We thank T. Neveselý for helpful discussions. **Funding:** We acknowledge financial support from the Westfälische Wilhelms-Universität Münster, the Deutsche Forschungsgemeinschaft (SFB 858), the Alexander von Humboldt Foundation (postdoctoral fellowship to J.J.M.), and the Verband der Chemischen Industrie (Kekulé Fellowship to T.M.). **Author contributions:** All authors contributed to the conceptualization of this study, the experimental design, and the interpretation of data. J.J.M. and R.G. directed the research. J.J.M. and R.G. wrote the manuscript with input from all authors. **Competing interests:** The authors declare no competing interests. **Data and materials availability:** X-ray structural data for ***Z*/*E*-8** (CCDC 1990167 and 1990168), ***Z*/*E*-16** (CCDC 1990169 and 1990170), and ***Z*-29** (CCDC 1990171) can be obtained free of charge from the Cambridge Crystallographic Data Centre (CCDC). All other experimental data are available in the main text or the supplementary materials.

SUPPLEMENTARY MATERIALS

science.sciencemag.org/content/369/6501/302/suppl/DC1
Materials and Methods
Figs. S1 to S11
Table S1
NMR Spectra
References (*47*–*90*)

13 March 2020; accepted 28 May 2020
10.1126/science.abb7235